Ultrafast Coulomb explosion of the NH_3 dimer, trimer, and tetramer in strong laser fields

Xinyu Zhang,[1,2] Xinning Zhao,[1,2] Hui Liu,[1,2] Zhongyu Yin,[1,2] Xiaoge Zhao,[1,2] Pan Ma,[1,2] Xiaokai Li,[1,2] Chuncheng Wang,[1,2] Qinxin Wang,[3,*] Sizuo Luo,[1,2,†] and Dajun Ding[1,2,‡]

[1]*Institute of Atomic and Molecular Physics, Jilin University, Changchun 130012, China*

[2]*Jilin Provincial Key Laboratory of Applied Atomic and Molecular Spectroscopy, Jilin University, Changchun 130012, China*

[3]*School of Electrical and Information Engineering, Jilin Engineering Normal University, Changchun 130012, China*

(Received 30 September 2023; accepted 16 January 2024; published 15 February 2024)

This study investigates the ultrafast fragmentation of ammonia clusters, $(NH_3)_n$ ($n = 2$, 3, and 4), by using ion-ion multibody coincidence measurements after interaction with a strong femtosecond laser. Specifically, the Coulomb explosion and proton transfer channels in the dimer, as well as the Coulomb explosion of tri- and tetramers, are assigned. The kinetic energy release distributions and Newton plots of each channel are extracted and analyzed. To gain further insights into the dissociation process, an *ab initio* molecular dynamics simulation was performed to uncover the dissociation mechanism. In addition, the stretching of clusters during the Coulomb explosion was identified using classical trajectory calculation combined with the genetic algorithm. This combined experimental and theoretical study holds significant importance in improving the understanding of the ultrafast Coulomb explosion process in molecular clusters.

DOI: 10.1103/PhysRevA.109.023112

I. INTRODUCTION

Molecules held together by various interactions, such as van der Waals and hydrogen bonds, play critical roles in chemistry and biology. The impact of these bonds on the structure and behavior of biomolecules and clusters has been extensively studied previously [1–5]. Recently, the fascinating research topics of Coulomb explosion (CE) and ultrafast proton transfer (PT) resulting from laser interactions with different molecular clusters have gained extensive attention [6–8]. Laser-induced Coulomb explosion imaging of clusters has shown promising capabilities in determining the structure of molecules and clusters [9–20]. Researchers have successfully determined the structure of various dimers, including $(H_2)_2$, N_2Ar, O_2Ar, and O_2Xe [21–23]. Investigations have also been conducted on the dissociation of N_2O dimer and two-body ring-breaking of Bz, where the influence of neighboring molecules on potential energy surfaces and the generation of new dissociation channels have been explored [10,11]. Neighboring molecules have been used as references to examine the lifetime between corresponding states and measure the charge distribution of molecular cations [11,14]. Additionally, observations of time-dependent ion pair yields and ultrafast rotation with a period time of 480 ± 60 fs have been made in the dicationic acetylene dimer [24]. Furthermore, details of sequential and concerted breakups from the CO dimer have been studied [13,25]. Despite these extensive studies, the structure and dissociation dynamics of clusters with different sizes is a lack of in-depth research; understanding the variations in behavior and properties could provide valuable insights into their structural evolutions.

The ionization and dissociation of small-sized NH_3 clusters have attracted increasing interest from both experimentalists and theoreticians as valuable sources of information for understanding complex phenomena [26–30]. The ionization processes of NH_3 dimers and larger clusters have been studied by electron impact [31], single-photon [32], and multiphoton ionization methods [33,34]. The stability of $(NH_3)_n$ ($n = 2$, 3, and 4) clusters has been explored, revealing that the line, triangle, and square structures are the most stable configurations [27,28,35]. Additionally, the tetramer cluster also has a "pyramidal" form, only about 1.3 kcal mol^{-1} above the most stable square one [36]. The ionization of NH_3 clusters $(NH_3)_n$ ($n = 2$–6) leads to the identification of a proton transfer reaction channel, and the timing of proton transfer is found to be dependent on the intermolecular distance between molecules [35]. The proton transfer in the NH_3 dimer involves the coordinated motion of several atoms, particularly changing its intermolecular distance and the rotation of the NH_2 moiety [37]. In the meantime, theoretical studies have primarily focused on the energies, structure, and proton transfer process of ionized NH_3 dimers [38–40], but only limited attention has been given to the structural dynamics after ionization.

This work investigates the ultrafast CE and PT processes of $(NH_3)_2^{2+}$, as well as the CE channels of $(NH_3)_3^{3+}$ and $(NH_3)_4^{4+}$ by means of the multibody coincidence measurements. The size-dependent nuclear dynamics during the dissociation process are studied experimentally and theoretically. Furthermore, the nuclear dynamics simulations for dimer, trimer, and tetramer reveal the underlying dissociation process for three clusters, and the bond stretching of clusters

*wangqx@jlenu.edu.cn
†luosz@jlu.edu.cn
‡dajund@jlu.edu.cn

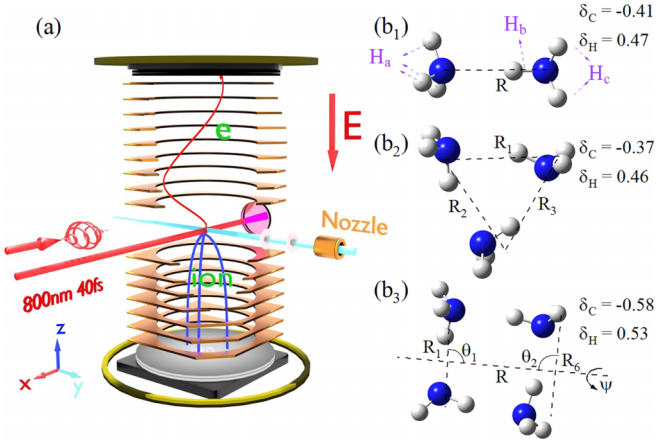

FIG. 1. The experimental setup is schematically illustrated in panel (a). Panels (b_1)–(b_3) are the stable neutral structures of $(NH_3)_2$, $(NH_3)_3$, and $(NH_3)_4$. The calculated distances between molecules are (b_1) $R = 3.3$ Å, (b_2) $R_1, R_2, R_3 = 3.2$ Å, and (b_3) $R_1, R_6, R = 3.2$ Å.

with three different sizes after ionization and before dissociation provides valuable information on structural change during fragmentation.

II. EXPERIMENTAL AND SIMULATION METHODS

The interaction of NH_3 clusters with a strong femtosecond laser beam (800 nm, 1 kHz, ~40 fs) is depicted in Fig. 1(a), where $(NH_3)_2$, $(NH_3)_3$, and $(NH_3)_4$, as shown in Figs. 1(b_1)–1(b_3), were generated by expanding a 1:3 mixture of NH_3 and Ar seeded gas through a supersonic jet at 1.8 bar. The experimental setup utilized cold-target recoil-ion-momentum spectroscopy [41,42], enabling multibody coincident measurements for clusters of different sizes. Additional details can be found in our previous publications [10,11,43]. To minimize potential variations in ionization probability among different isomers of NH_3 clusters, a circularly polarized laser was employed [44]. The resulting ionic fragments were extracted towards a time- and position-sensitive particle detector using a static electric field, performing coincidence measurements. The count rate per laser pulse was limited to less than 0.4. The distinction between the CE and PT channels was based on the ratio R, defined as $R = P_x/C_x + P_y/C_y + P_z/C_z$, where $P_{x,y,z}$ are the total momentum and $C_{x,y,z}$ are the center-of-mass (c.m.) momentum along the x, y, and z axes. The R value gives the difference in momentum coincidence between the channel's total momentum and c.m. momentum, representing the momentum coincidence degree. $R = 0$ indicates the best coincidence degree for the signals.

All the simulations were carried out under the GAUSSIAN 09 [45] software package. The most stable neutral structures were optimized with the MP2 method under the basis set 6-311 + +g(d, p). The structures of CE channels from $(NH_3)_3^3+$ and $(NH_3)_4^4+$ were reconstructed using classical trajectory calculation combined with the genetic algorithm [44]. The dynamic simulations were conducted using *ab initio* molecular dynamics (AIMD) simulations. For these calculations, we considered the optimized structures starting from the global-energy minimum geometry [see Figs. 1(b_1)–1(b_3)]. The AIMD simulations were performed in two steps: In the first step, the initial conditions, including the geometries and velocities of every atom, were based on the neutral structure. The initial conditions were sampled using Born-Oppenheimer molecular dynamics, in which the populations of the initial vibrational states were determined by Boltzmann distributions with the sampling temperature set at 50 K. In the second step, the dynamics simulations of the doubly charged dimer, the trication trimer, and the tetramer losing four electrons, all start from the same structures as neutral systems. Each molecule shares one charge after removing electrons from the highest occupied molecular orbital of the monomers, and the charge distribution (δ) on each atom is given in Figs. 1(b_1)–1(b_3). The dynamical simulations were performed using the extended Lagrangian molecular dynamics scheme, adopting the atom-centered density matrix propagation method [46–48]. We employed the B97XD method, which is a long-range corrected hybrid density-functional theory, with the 6-31g basis set. Propagation was performed for 1000 fs with a time step of 1 fs.

III. RESULTS AND DISCUSSION

The CE and PT channels of $(NH_3)_n^{n+}$ ($n = 2$, 3, and 4) were measured coincidentally as depicted by the time-of-flight coincidence maps in Figs. 2(a)–2(c):

$$(NH_3)_2^{2+} \rightarrow NH_3^+ + NH_3^+, \quad (1)$$

$$(NH_3)_2^{2+} \rightarrow NH_2^+ + NH_4^+, \quad (2)$$

$$(NH_3)_3^{3+} \rightarrow NH_3^+ + NH_3^+ + NH_3^+, \quad (3)$$

$$(NH_3)_4^{4+} \rightarrow NH_3^+ + NH_3^+ + NH_3^+ + NH_3^+. \quad (4)$$

The coincident time-of-flight of ionic fragments provided valuable insights into the dynamics of $(NH_3)_2^{2+}$. We can identify and separate both a direct CE channel (1) and a PT channel (2) from dimers. The leaf-shaped structure seen in Fig. 2(b) corresponds to the three-body CE channel (3) from the trimer, while the four-body CE channel (4) from the tetramer shown in Fig. 2(c) exhibited a slightly, broader leaflike shape. Figures 2(d)–2(f) present both experimentally measured and theoretically simulated kinetic energy release (KER) spectra for the two-, three-, and four-body dissociation channels. In the two-body CE channel of $(NH_3)_2^{2+}$, a peak KER value centered at 3.9 eV was observed [Fig. 2(d)], and this value agrees with the observation from electron collision-induced CE [26]. The KER of the PT channel from $(NH_3)_2^{2+}$ displayed a two-peak distribution, with the main peak aligned well with the CE channel, and a secondary peak accounting for half the counts of the main peak, which appears at 4.6 eV. However, there is one peak distribution centered around 4.0 eV observed in the electron collision PT channel [26]. This secondary peak is most likely generated by the sequential ionization of dimers during PT. After the dimer is single-ionized by the laser, the structure of the cation deforms, causing the distance of the N-H bond to decrease by 0.58 Å compared to the neutral NH_3 dimer [37], and then the second electron is ionized sequentially by the laser pulse. And the energy release also comes from the proximity of the

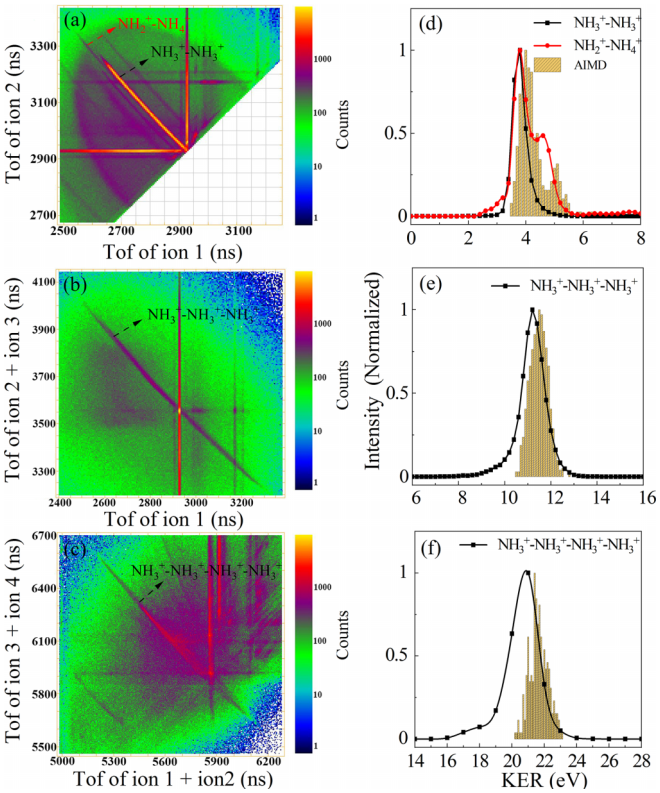

FIG. 2. Time-of-flight coincidence map corresponding to (a) the two-body dissociation paths of $(NH_3)_2^{2+}$, (b) the three-body dissociation channel from $(NH_3)_3^{3+}$, and (c) the four-body dissociation channel from $(NH_3)_4^{4+}$. (d) The KER spectra of the CE channel (1) (represented by the black square line) and the PT channel of channel (2) (represented by the red circle line) from $(NH_3)_2^{2+}$. Panels (e) and (f) display the KER of CE channels (3) and (4) from $(NH_3)_3^{3+}$ and $(NH_3)_4^{4+}$. The yellow slash histogram is the obtained KER distributions from the theoretical simulation of $(NH_3)_2^{2+}$, $(NH_3)_3^{3+}$, and $(NH_3)_4^{4+}$.

two molecules before PT dissociation. Due to the shortened distance between two molecules, the resulting KER becomes larger when the CE occurs in the double-charged states. The small peak at 5.1 eV of the simulated results originates from the proximity of the two NH_3 molecules before dissociation in the CE channel of the dimer, while the main peak at 3.9 eV corresponds to the direct dissociation of the two fragments. In the three-body CE of $(NH_3)_3^{3+}$, the KER spectrum [Fig. 2(e)] exhibited a single-peak structure with the most probable energy appearing at 11.2 eV. The four-body CE channel of $(NH_3)_4^{4+}$, shown in Fig. 2(f), has the peak energy closely located at 20.8 eV. The KER distribution obtained from theoretical simulations closely matched the experimental values but was slightly larger. The obtained most probable energies for three channels are 4.0, 11.4, and 21.6 eV, as depicted in the column distribution in Figs. 2(d)–2(f). An asymmetric distribution towards lower energies in the KER spectra in the measured results may be caused by the non-Coulomb interactions; the interaction of three-body and four-body fragments and the population of vibrational states after ionization will be more complicated [49,50], leading to a larger KER shift spread. The agreement demonstrates the reliability of the simulation and can reveal the underlying dissociation dynamics.

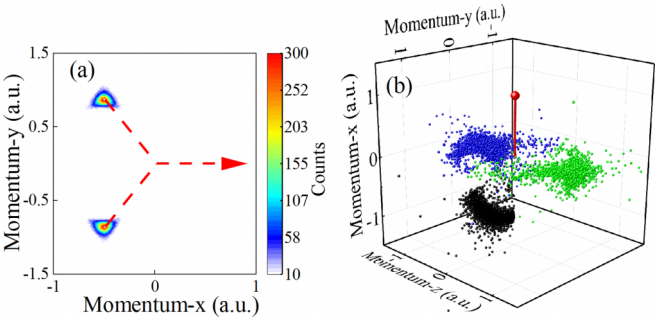

FIG. 3. Panels (a) and (b) are the experimental Newton plots obtained for the three-body and four-body dissociation channels.

The experimental Newton diagrams of $(NH_3)_n$ ($n = 3$ and 4) clusters are presented in Fig. 3. In the three-body CE channel, the momenta of one of the NH_3^+ ions were normalized to 1 atomic unit (a.u.) using a normalization factor of 89. During the three-body CE process, the average Coulomb repulsive force resulted in a triangular momentum distribution in the Newton diagram, as shown in Fig. 3(a), which indicates that the three-body CE from triple-charged trimers occurs through a concerted dissociation process. In the four-body CE channel [Fig. 3(b)], the momentum distribution was normalized to one of the NH_3^+ ions (red ball), and the normalization factor was 105. The large, uniform momentum distribution suggests a concerted dissociation process, while a small portion of the circular distribution may arise from sequential dissociation.

To interpret the CE dynamics, the simulations provided time-dependent c.m. distances between each fragment, as presented in Figs. 4(a)–4(c), offering direct indications for the dissociation process. In the CE channel from $(NH_3)_2^{2+}$, the distance between two NH_3 molecules shows a monotonic increase with the evolution time as shown in Fig. 4(a), indicating that the system would dissociate into two intact NH_3^+ ions once ionized to dication states. Before the PT process occurs, there are also some trajectories that exhibit a long time-delayed structural oscillatory process, resulting in the bond length asymptotically approaching 0.5 a.u. in Fig. 4(a). The PT process of $(NH_3)_2^{2+}$ occurred through two dissociation pathways: (i) Initially, two separate N atoms from NH_3^+ formed a covalent bond, followed by the breaking of the N-N bond after a period of vibration and rotation. Subsequently, one of H_a or H_c transferred to the neighbor molecule as marked in Fig. 1(b_1), resulting in the formation of protonated products NH_2^+ and NH_4^+. (ii) Another process involved the direct transfer of H_b onto another N atom, leading to the formation of protonated products within around 10 fs. The fast separation of $(NH_3)_3^{3+}$ in Fig. 4(b) indicated that all trajectories began to dissociate at 50 fs, with three ions dissociating in three directions simultaneously due to the Coulomb repulsive force of the triangular structure. In Fig. 4(c), two dissociation pathways were observed for the CE of $(NH_3)_4^{4+}$. In one pathway, two $NH_3 \cdot NH_3^{2+}$ intermediates were first generated, and the further four-body dissociation occured after 200 fs. In the other pathway, all four ions began to dissociate at the same time at around 80 fs. The simulations show that the CE of clusters with different sizes and structures present very unique dynamics, which is very sensitive to the initial structures.

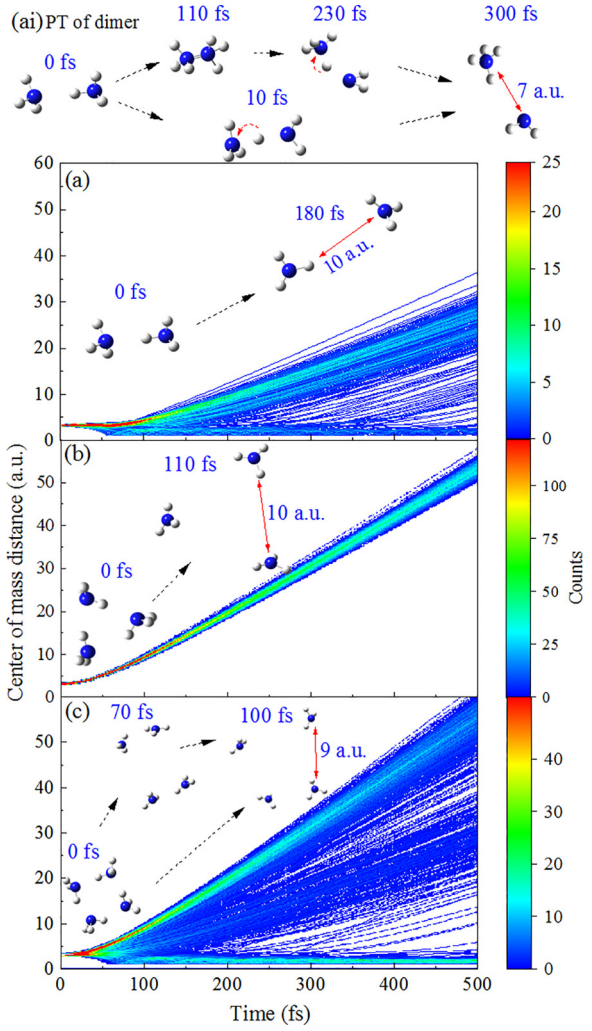

FIG. 4. Panels (a)–(c) are the time-dependent distances between each fragment for the fragmentation of $(NH_3)_n^{n+}$ ($n = 2$, 3, and 4) from the AIMD simulations. Panel (ai) shows the fragmentation trajectory from the PT channel of the dimer. The cartoon plots inside panels (a)–(c) give the most probable fragmentation trajectories from CE of $(NH_3)_2^{2+}$, $(NH_3)_3^{3+}$, and $(NH_3)_4^{4+}$.

The reconstructed experimental intermolecular bond lengths of three clusters are shown in Fig. 5. The bond length can be directly calculated from the measured KER when assuming the CE and point charge approximation (PCA). Actually, the potential energy surface may be distorted under the PCA [49], but the effect is much smaller than the stretching of the bond length. For the CE channel of the dimer, the measured distance between two NH_3 is 3.72 Å. In the PT channel, there are two most probable KER peaks observed, which correspond to the bond lengths of 3.7 Å and a much shorter one of 3.55 Å. The measured distance between molecules after dissociation reveals the underlying mechanism of how PT happens. One of the PT channels occurs very fast before the structure changes, while the other one takes some time and leads to a strong structural deformation. These are also observed in the AIMD simulation shown in Fig. 4(a). The measured distances between molecules for trimers and tetramers are mean values calculated by following the CE and the point charge approximation, and the obtained values are 3.85 and 4.15 Å for the trimer and the tetramer as shown in Fig. 5(a).

In order to acquire structural information of each distance between molecules for trimers and tetramers through a three-body and a four-body coincidence measurement, the genetic algorithm and classical trajectory Coulomb explosion simulation combination method proved to be a highly effective tool for structural reconstruction. Figures 5(b)–5(e) illustrate the reconstructed outcomes pertaining to the distances between molecules derived from the momenta observed in three-body and four-body coincidences. The reconstructed bond lengths between molecules within the trimer, obtained from three-body fragments denoted as R_1, R_2, and R_3, were determined to be 3.85 Å, as depicted in Fig. 5(b). These values were slightly longer than those of the neutral ground-state structure ($R = 3.2$ Å). For the four-body system, the results were as follows: $R_1 = 3.8$ Å, $R_2 = 4.1$ Å, $R_3 = 4.5$ Å, $R_4 = 4.4$ Å, $R_5 = 4.1$ Å, and $R_6 = 3.8$ Å, as presented in Fig. 5(d). Here, R_1, R_2, R_5, and R_6 are adjacent bond lengths, while R_3 and R_4 indicate diagonal distances as marked in Fig. 5(e). These reconstructed values significantly exceeded those from the neutral tetramer. In all three cluster sizes, distinct degrees of bond length elongation and structural deformations were observed during the Coulomb explosion process. Thus, the measured KER values lower than the simulation results are caused by these structural transformations as well as by the ionization mechanism of the pulsed laser during light absorption, as depicted in Figs. 2(d)–2(f).

In the meantime, the trimer's equilateral triangle structure, as illustrated in Fig. 5(c), leads to a swift and symmetrical dissociation of its three-body fragments, as depicted in Fig. 4(b). Figure 5(e) vividly portrays the substantial structural elongation within the four-body system, facilitating the emergence of the $NH_3 \cdot NH_3^{2+}$ intermediate species, as seen in Fig. 4(c). Analyzing the reconstructed results, particularly in the vicinity of coordinates [$\theta_1 = 50°$, 130°, $\theta_2 = 50°$, 130°, $\psi = 20°$, as defined in Fig. 1(b_3)], we discern that two angular distributions indicate the ionization excitation to structural changes, suggesting the existence of "pyramidal" isomers within the four-body system [36]. Furthermore, the energy-angle correlation depicted in Fig. 5(f) reveals intriguing patterns for the evidence of the existence of two isomers. Apart from a concentration of data at $\theta_{12} = 94°$ associated with an energy of approximately 5.2 eV from the stable square isomer, the angle distribution between 110° and 180° is notably influenced by the presence of the pyramidal isomer, whereas the θ_{12} angle is defined in the inset of Fig. 5(f) and shows the angle of momentum between two fragments. The bond length of the pyramidal structure is longer than that of the square structure, leading to the existence of a smaller KER at 17 eV in Fig. 2(f). This analysis underscores the profound structural transformations occurring within the clusters before dissociation, underscoring the dynamic nature of the dissociation processes within molecular clusters.

IV. CONCLUSION

Ultrafast Coulomb explosion of $(NH_3)_n$ ($n = 2$, 3, and 4) clusters were investigated using mulitbody coincidence

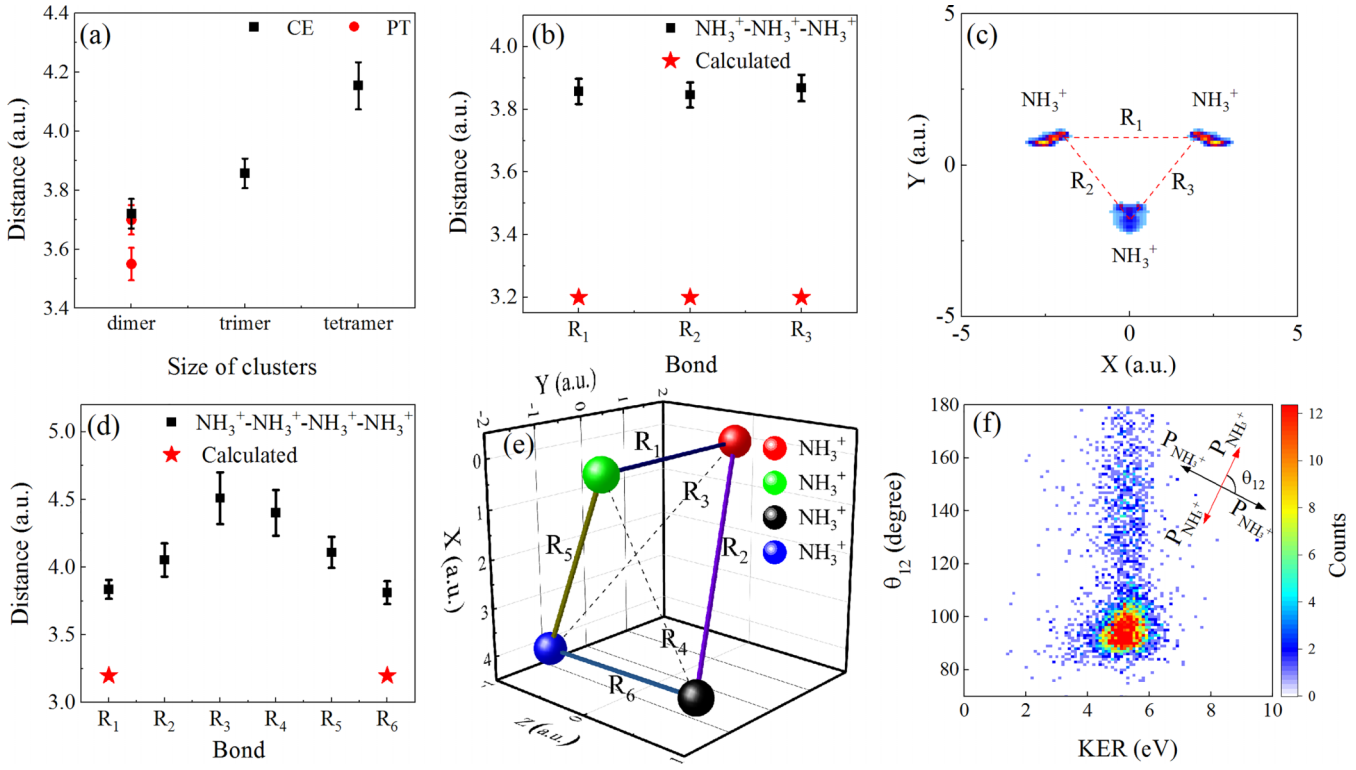

FIG. 5. (a) Experimentally measured distance between molecules from four dissociation channels. (b) Reconstructed distance between three molecules from the three-body dissociation channel. (c) Reconstructed structure of trimer from the three-body coincidence measurement. (d) Reconstructed distance between four molecules from the four-body dissociation channel. (e) Reconstructed structure of tetramer from the four-body coincidence data. (f) Experimental energy-angle correlation map for channel (4), where the kinetic energy comes from one of the four indistinguishable fragments. The red stars in panels (b) and (d) are the calculated distance of neutral structures, and the angle θ_{12} is marked inside the figure.

measurement combined with the *ab initio* molecular dynamic simulation and the genetic algorithm reconstruction. Two dissociation mechanisms of the PT channel were identified from the dimer. In the case of tri- and tetramer clusters, the Coulomb explosion primarily occurred through a concerted dissociation process. Our theoretical simulations revealed a rapid direct Coulomb explosion channel and two PT channels during the two-body dissociation of $(NH_3)_2^{2+}$. Additionally, we observed that $(NH_3)_3^{3+}$ exhibited simultaneous separation into three ions within just 50 fs. In the case of the four-body Coulomb explosion of $(NH_3)_4^{4+}$, we identified both a direct dissociation channel and a channel involving intermediate products. Our reconstruction results pointed to bond stretching occurring after ionization but before the final fragmentation. This study on the dissociation mechanisms within clusters of varying sizes provides valuable insights that can guide future research in the field of molecular clusters.

ACKNOWLEDGMENTS

This work was supported by the National Natural Science Foundation of China (Grants No. 12074143, No. 12004135, No. 92250306, and No. 12134005), the National Basic Research Program of China (Grant No. 2019YFA0307701), and the Fundamental Research Funds for the Central Universities.

APPENDIX: RECONSTRUCTION STRUCTURES FROM $(NH_3)_3^{3+}$ AND $(NH_3)_4^{4+}$

In this section, we provide a detailed explanation of the reconstruction process utilized to determine the structure in coordinate space based on the measured momenta acquired during the Coulomb explosion. We conducted Coulomb explosion simulations for various initial geometries by numerically solving Newton's equations of motion, and subsequently compared the simulated momenta with the measured ones using a differential evolution algorithm to adjust the initial structure. To assess the goodness of fit, we introduced a parameter (η) defined as follows:

$$\eta = \sum_{i=1}^{N} \left| p_i^e - p_i^s \right| + \sum_{j>i}^{N} \left| \delta p_{ij}^e - \delta p_{ij}^s \right|,$$

where p_i is the magnitude of the ith ion momentum vector, and δp_{ij} is the magnitude of the momenta difference of the ith and jth ions. Superscripts e and s indicate the experiment and the simulation, respectively. It is worth noting that the accuracy of the reconstruction method has been previously demonstrated in our study [44]. In the case of the three-body breakup, $N = 3$. By comparing the magnitudes of the vectors rather than the vectors themselves, we eliminated rotational degrees of freedom, effectively reducing the number of parameters required for the fitting process. The trimer

structure is characterized by three bond lengths (R_1, R_2, and R_3), as depicted in Fig. 1(b_2). Only structures with an optimized η value below 1% were considered. During the fitting process, intermolecular bond lengths were constrained within the range of 1 to 7 a.u. The initial structure in our Coulomb explosion simulation was assumed to be at rest. In reality, however, the ions acquire momenta due to the recoil of the emitted electrons upon ionization. These initial momenta, which are relatively small (less than 1 a.u.), were neglected in our simulation. For the four-body breakup ($N = 4$), the complexity of reconstruction increases with the number of ions involved. In this case, six-dimensional parameters were required to describe the structure of a group of four molecules, considering each molecule as a particle. The tetramer structure is characterized by three bond lengths (R_1, R_6, and R) and three angles (θ_1, θ_2, and ψ) as depicted in Fig. 1(b_3). During the fitting process, intermolecular bond lengths were restricted within the following ranges: R_1, 1–10 a.u.; R_6, 1–10 a.u.; and R 2–30 a.u., respectively. The angles were considered in the range of 0° to 180°.

[1] X. Gong, S. Heck, D. Jelovina, C. Perry, K. Zinchenko, R. Lucchese, and H. J. Wörner, Attosecond spectroscopy of size-resolved water clusters, Nature (London) **609**, 507 (2022).

[2] J. Zhou, X. Yu, S. Luo, X. Xue, S. Jia, X. Zhang, Y. Zhao, X. Hao, L. He, C. Wang, D. Ding, and X. Ren, Triple ionization and fragmentation of benzene trimers following ultrafast intermolecular Coulombic decay, Nat. Commun. **13**, 5335 (2022).

[3] X. Ren, E. Wang, A. D. Skitnevskaya, A. B. Trofimov, K. Gokhberg, and A. Dorn, Experimental evidence for ultrafast intermolecular relaxation processes in hydrated biomolecules, Nat. Phys. **14**, 1062 (2018).

[4] E. Wang, X. Ren, W. Baek, H. Rabus, T. Pfeifer, and A. Dorn, Water acting as a catalyst for electron-driven molecular breakup of tetrahydrofuran, Nat. Commun. **11**, 2194 (2020).

[5] I. Compagnon, R. Antoine, D. Rayane, M. Broyer, and P. Dugourd, Vibration induced electric dipole in a weakly bound molecular complex, Phys. Rev. Lett. **89**, 253001 (2002).

[6] C. Lu, M. Shi, S. Pan, L. Zhou, J. Qiang, P. Lu, W. Zhang, and J. Wu, Electron transfer in strong-field three-body fragmentation of $ArKr_2$ trimers, J. Chem. Phys. **158**, 094302 (2023).

[7] L. Wei, C.-S. Lam, Y. Zhang, B. Ren, J. Han, B. Wang, Y. Zou, L. Chen, K.-C. Lau, and B. Wei, Isomerization dynamics in the symmetric and asymmetric fragmentation of ethane dications, J. Phys. Chem. Lett. **12**, 5789 (2021).

[8] C. Zhang, J. Lu, T. Feng, and H. Rottke, Proton transfer dynamics following strong-field ionization of the water dimer, Phys. Rev. A **99**, 053408 (2019).

[9] J. Gagnon, K. F. Lee, D. M. Rayner, P. B. Corkum, and V. R. Bhardwaj, Coincidence imaging of polyatomic molecules via laser-induced Coulomb explosion, J. Phys. B: At. Mol. Opt. Phys. **41**, 215104 (2008).

[10] X. Yu, X. Zhang, X. Hu, X. Zhao, D. Ren, X. Li, P. Ma, C. Wang, Y. Wu, S. Luo, and D. Ding, Femtosecond time-resolved neighbor roles in the fragmentation dynamics of molecules in a dimer, Phys. Rev. Lett. **129**, 023001 (2022).

[11] X. Zhang, X. Zhao, H. Liu, X. Yu, D. Ren, X. Zhao, X. Li, C. Wang, Q. Wang, S. Luo, and D. Ding, Revealing the two-body ring-breaking dynamics of benzene in the $(C_6H_6)_2$, C_6H_6Ar, and C_6H_6Kr dimers, Phys. Rev. A **107**, 043115 (2023).

[12] I. Last and J. Jortner, Dynamics of the Coulomb explosion of large clusters in a strong laser field, Phys. Rev. A **62**, 013201 (2000).

[13] X. Ding, M. Haertelt, S. Schlauderer, M. S. Schuurman, A. Yu. Naumov, D. M. Villeneuve, A. R. W. McKellar, P. B. Corkum, and A. Staudte, Ultrafast dissociation of metastable CO^{2+} in a dimer, Phys. Rev. Lett. **118**, 153001 (2017).

[14] X. Yu, X. Hu, J. Zhou, X. Zhang, X. Zhao, S. Jia, X. Xue, D. Ren, X. Li, Y. Wu, X. Ren, S. Luo, and D. Ding, Measuring charge distribution of molecular cations by an atomic Coulomb probe microscope, Chin. Phys. Lett. **39**, 113301 (2022).

[15] X. Li, X. Yu, P. Ma, X. Zhao, C. Wang, S. Luo, and D. Ding, Ultrafast Coulomb explosion imaging of molecules and molecular clusters, Chin. Phys. B **31**, 103304 (2022).

[16] C. A. Schouder, A. S. Chatterley, J. D. Pickering, and H. Stapelfeldt, Laser-induced Coulomb explosion imaging of aligned molecules and molecular dimers, Annu. Rev. Phys. Chem. **73**, 323 (2022).

[17] R. Boll, J. M. Schäfer, B. Richard, K. Fehre, G. Kastirke, Z. Jurek, M. S. Schöffler, M. M. Abdullah, N. Anders, T. M. Baumann, S. Eckart, B. Erk, A. De Fanis, R. Dörner, S. Grundmann, P. Grychtol, A. Hartung, M. Hofmann, M. Ilchen, L. Inhester *et al.*, X-ray multiphoton-induced Coulomb explosion images complex single molecules, Nat. Phys. **18**, 423 (2022).

[18] X. Zhao, T. Xu, X. Yu, D. Ren, M. Li, X. Zhang, X. Li, P. Ma, D. Zhang, C. Wang, Q. Wang, X. Hu, S. Luo, Y. Wu, J. Wang, and D. Ding, Probing electron localization during molecular dissociation by femtosecond strong-field ion momentum spectroscopy, Commun. Phys. **6**, 124 (2023).

[19] S. W. Crane, J. W. L. Lee, M. N. R. Ashfold, and D. Rolles, Molecular photodissociation dynamics revealed by Coulomb explosion imaging, Phys. Chem. Chem. Phys. **25**, 16672 (2023).

[20] C. Cheng, L. J. Frasinski, G. Mogol, F. Allum, A. J. Howard, D. Rolles, P. H. Bucksbaum, M. Brouard, R. Forbes, and T. Weinacht, Multiparticle cumulant mapping for Coulomb explosion imaging, Phys. Rev. Lett. **130**, 093001 (2023).

[21] A. Khan, T. Jahnke, S. Zeller, F. Trinter, M. Schöffler, L. P. H. Schmidt, R. Dörner, and M. Kunitski, Visualizing the geometry of hydrogen dimers, J. Phys. Chem. Lett. **11**, 2457 (2020).

[22] C. Wu, C. Wu, D. Song, H. Su, X. Xie, M. Li, Y. Deng, Y. Liu, and Q. Gong, Communication: Determining the structure of the N_2Ar van der Waals complex with laser-based channel-selected Coulomb explosion, J. Chem. Phys. **140**, 141101 (2014).

[23] J. Wu, M. Kunitski, L. Ph. H. Schmidt, T. Jahnke, and R. Dörner, Structures of N_2Ar, O_2Ar, and O_2Xe dimers studied by Coulomb explosion imaging, J. Chem. Phys. **137**, 104308 (2012).

[24] J. Zhou, C. He, M.-M. Liu, E. Wang, S. Jia, A. Dorn, X. Ren, and Y. Liu, Real-time observation of ultrafast molecular rotation in weakly bound dimers, Phys. Rev. Res. **3**, 023050 (2021).

[25] P. Song, X. Wang, C. Meng, W. Dong, Y. Li, Z. Lv, D. Zhang, Z. Zhao, and J. Yuan, Dynamics of three-particle fragmentation

of $(CO_2)_2^{3+}$ ions produced by intense femtosecond laser fields, Phys. Rev. A **99**, 053427 (2019).

[26] J. Zhou, M. Belina, S. Jia, X. Xue, X. Hao, X. Ren, and P. Slavek, Ultrafast charge and proton transfer in doubly ionized ammonia dimers, J. Phys. Chem. Lett. **13**, 10603 (2022).

[27] L. Yu and Z.-Z. Yang, Study on structures and properties of ammonia clusters $(NH_3)_n$ ($n = 1$–5) and liquid ammonia in terms of *ab initio* method and atom-bond electronegativity equalization method ammonia-8*P* fluctuating charge potential model, J. Chem. Phys. **132**, 174109 (2010).

[28] S. A. Kulkarni and R. K. Pathak, *Ab initio* investigations on neutral clusters of ammonia: $(NH_3)_n$ ($n = 2$–6), Chem. Phys. Lett. **336**, 278 (2001).

[29] J. S. Lee and S. Y. Park, *Ab initio* study of $(NH_3)_2$: Accurate structure and energetics, J. Chem. Phys. **112**, 230 (2000).

[30] N. V. Kryzhevoi and L. S. Cederbaum, Nonlocal effects in the core ionization and Auger spectra of small ammonia clusters, J. Phys. Chem. B **115**, 5441 (2011).

[31] U. Buck, H. Meyer, D. Nelson, G. Fraser, and W. Klemperer, Fragmentation of NH_3 dimers by electron impact ionization, J. Chem. Phys. **88**, 3028 (1988).

[32] F. Dong, S. Heinbuch, J. J. Rocca, and E. R. Bernstein, Dynamics and fragmentation of van der Waals clusters: $(H_2O)_n$, $(CH_3OH)_n$, and $(NH_3)_n$ upon ionization by a 26.5 eV soft x-ray laser, J. Chem. Phys. **124**, 224319 (2006).

[33] S. A. Buzza, S. Wei, J. Purnell, and A. W. Castleman, Jr., Formation and metastable decomposition of unprotonated ammonia cluster ions upon femtosecond ionization, J. Chem. Phys. **102**, 4832 (1995).

[34] H. Shinohara and N. Nishi, Multiphoton ionization mass spectroscopic detection of ammonia clusters, Chem. Phys. Lett. **87**, 561 (1982).

[35] H. Tachikawa, Intramolecular reactions in ionized ammonia clusters: A direct *ab initio* molecular dynamics study, J. Phys. Chem. A **124**, 1903 (2020).

[36] A. Malloum, J. J. Fifen, Z. Dhaouadi, S. G. N. Engo, and N.-E. Jaidane, Structures and relative stabilities of ammonia clusters at different temperatures: DFT *vs. ab initio*, Phys. Chem. Chem. Phys. **17**, 29226 (2015).

[37] J. Chalabala and P. Slavíček, Nonadiabatic dynamics of floppy hydrogen bonded complexes: The case of the ionized ammonia dimer, Phys. Chem. Chem. Phys. **18**, 20422 (2016).

[38] S. Tomoda and K. Kimura, Equilibrium structure and two kinds of dissociation energy of the ammonia dimer cation H_3NH^+…NH_2, Chem. Phys. Lett. **121**, 159 (1985).

[39] S. Tomoda, Ionization of the ammonia dimer: Proton transfer in the ionic state, Chem. Phys. **110**, 431 (1986).

[40] H. Kim and H. M. Lee, Ammonia-water cation and ammonia dimer cation, J. Phys. Chem. A **113**, 6859 (2009).

[41] R. Dörner, V. Mergel, O. Jagutzki, L. Spielberger, J. Ullrich, R. Moshammer, and H. Schmidt-Böcking, Cold target recoil ion momentum spectroscopy: A 'momentum microscope' to view atomic collision dynamics, Phys. Rep. **330**, 95 (2000).

[42] J Ullrich, R Moshammer, A Dorn, R Dörner, L Ph H Schmidt, and H Schmidt-Böcking, Recoil-ion and electron momentum spectroscopy: Reaction-microscopes, Rep. Prog. Phys. **66**, 1463 (2003).

[43] S. Luo, J. Liu, X. Li, D. Zhang, X. Yu, D. Ren, M. Li, Y. Yang, Z. Wang, P. Ma, C. Wang, J. Zhao, Z. Zhao, and D. Ding, Revealing molecular strong field autoionization dynamics, Phys. Rev. Lett. **126**, 103202 (2021).

[44] X. Yu, X. Zhao, Z. Wang, Y. Yang, X. Zhang, P. Ma, X. Li, C. Wang, X. Xu, C. Wang, D. Zhang, S. Luo, and D. Ding, Determining the stereo configuration of carbonyl sulfide dimers using Coulomb-explosion imaging, Phys. Rev. A **104**, 053104 (2021).

[45] M. J. Frisch, G. W. Trucks, H. B. Schlegel, G. E. Scuseria, M. A. Robb, J. R. Cheeseman, G. Scalmani, V. Barone, B. Mennucci, G. A. Petersson, H. Nakatsuji, M. Caricato, X. Li, H. P. Hratchian, A. F. Izmaylov, J. Bloino, G. Zheng, J. L. Sonnenberg, M. Hada, M. Ehara *et al.*, Gaussian 09, Revision D.01 (Gaussian, Inc., Wallingford CT, 2013).

[46] Y. Wang, E. Wang, J. Zhou, A. Dorn, and X. Ren, Formation of covalently bound $C_4H_4^{4+}$ upon electron-impact ionization of acetylene dimer, J. Chem. Phys. **154**, 144301 (2021).

[47] H. B. Schlegel, J. M. Millam, and S. S. Iyengar, *Ab initio* molecular dynamics: Propagating the density matrix with Gaussian orbitals, J. Chem. Phys. **114**, 9758 (2001).

[48] H. B. Schlegel, S. S. Iyengar, and X. Li, *Ab initio* molecular dynamics: Propagating the density matrix with Gaussian orbitals. III. Comparison with Born–Oppenheimer dynamics, J. Chem. Phys. **117**, 8694 (2002).

[49] C. A. Schouder, A. S. Chatterley, L. B. Madsen, F. Jensen, and H. Stapelfeldt, Laser-induced Coulomb-explosion imaging of the CS_2 dimer: The effect of non-Coulombic interactions, Phys. Rev. A **102**, 063125 (2020).

[50] S. Chelkowski, P. B. Corkum, and A. D. Bandrauk, Femtosecond Coulomb explosion imaging of vibrational wave functions, Phys. Rev. Lett. **82**, 3416 (1999).